MAS NMR study of the photoreceptor phytochrome

Rohmer, T.

Chapter 2

CP/MAS NMR study on microcrystalline phycocyanobilin

2.1 Introduction

Bilins are linear tetrapyrroles. This class of compounds has been named as bile pigments of mammals, however, they are also found in lower vertebrates, invertebrates as well as in red algae and green plants. In mammals, tetrapyrroles are generated as products of heme catabolism, which results in the formation of the linear tetrapyrroles biliverdin and bilirubin [69]. In plants and algae, linear tetrapyrrolic moieties are present, for example, as cofactors of the photoreceptor Phy and the cyanobacterial light-harvesting phycobiliproteins. One member of the bilin family, PCB (Fig. 2.1), is the chromophore of the antenna protein phycocyanin [70] as well as of the cyanobacterial phytochrome Cph1 [71].

Tetrapyrrole moieties are known to adopt a helical structure in solution [23, 72, 73]. In the late 1990's, Schaffner and co-workers have studied PCB in $CDCl_3$:Pyridine-d_5 and CD_3OD solutions, where it adopts a helically coiled form with an (all-*Z*, all-*syn*)-conformation [24]. In the case of phycocyanobilin dimethyl ester, two types of coiled tetrapyrrolic moieties are present in $CDCl_3$ and CD_2Cl_2 solutions at low concentration: a helically coiled form and another form characterized by some degree of stretching of the chain.

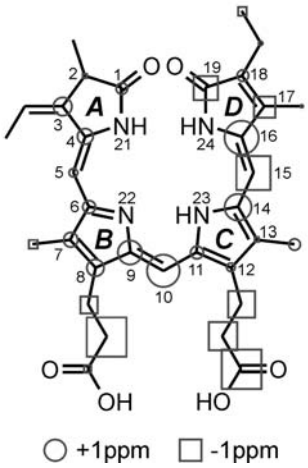

Figure 2.1: Structure of phycocyanobilin in the *ZZZsss* geometry as determined in solution [24]. The differences in the ^{13}C chemical shifts between the A and B forms (σ_{B}-σ_{A}) are projected on the chemical structure.

Upon increase in concentration, the relative proportion of the stretched form decreases and dimers of helically coiled PCBE appear [74]. In the same work, also a partial set of ^{13}C assignments has been obtained.

Semi-empirical AM1 studies [25, 75] and transient-grating spectroscopy [76] on PCB have proposed that three families of ground-state conformers coexist in solution. The predominant family adopts a cyclic-helical conformation (*ZZZsss*) with two types of helices, a right-handed (**P**) and a left-handed (**M**) helix [23, 24]. The other minimum-energy structures are obtained by rotation around the single bond of the C5 and C10 methine bridges, leading to two partially extended *ZZZass* and *ZZZsas* conformations [25, 75]. However, a precise structural analysis of PCB and its dimethyl ester is difficult because of the dynamics between the many possible conformations, the complex solvent effects and the limited solubility in most common solvents. Therefore, a structural analysis in the solid state provides a possibility to overcome these problems.

Although the 1,19-dioxobilin family has been intensively studied by X-ray crystallography [77], no description of PCB in its crystalline state is available yet. MAS NMR [78] has been developing to a method allowing for structure determination of aggregates [79], disordered systems [80] and membrane

proteins [81, 82]. In this chapter, the structure of PCB in microcrystalline samples is analyzed by a combination of MAS NMR and quantum mechanical calculations.

2.2 Results

2.2.1 ^{13}C chemical shift assignment

The one-dimensional ^{13}C CP/MAS spectrum of PCB in its microcrystalline state is shown in Figure 2.2. Although PCB contains 33 carbon atoms, around 45 centerbands are observable in the ^{13}C CP/MAS spectrum. The spinning sidebands have been determined by experiments at other spinning frequencies (data not shown) and are indicated with asterisks. PCB contains 11 aliphatic carbons in the side-chains, while 14 signals arising from the aliphatic carbons are observed between 0 and 40 ppm. Similarly, the carbonyl/carboxyl region of the spectrum (170-180 ppm) shows 6 signals that correspond with the response from 4 carbonyl carbons. In the aromatic region of the spectrum between 120 and 160 ppm, the signals of the pyrrole carbons strongly overlap, making the determination of the exact number of carbons involved difficult. On the other hand, in the region of methine carbons (120-80 ppm), at least five signals appear.

Liquid-state ^{1}H-^{13}C heteronuclear single quantum coherence and heteronuclear multiple bond correlation NMR spectra obtained in CD_3OD are shown in Appendix A (Fig. A.1). An almost complete set of ^{13}C assignments is presented in Table 2.1. While the solution spectra do not show any doubling of signal, the solid-state NMR data exhibit resonances which are clearly split. For instance, the liquid-state NMR spectrum of PCB exhibits signals at 98.3, 113.4 and 176.0 ppm, which were assigned to C15, C10 and C19, respectively. Similar resonances are present in the CP/MAS spectrum, however, these resonances are clearly doubled (96.0 and 93.6, 114.5 and 112.2, 173.7 and 172.0 ppm). The Lorentzian deconvolution of these doubled resonances (data not shown) reveals that the peak area ratios of all these doublets are 1:1. The observation of a consistent set of doubled signals in a 1:1 area ratio in the 1D CP/MAS NMR spectrum provides convincing evidence for the presence of two inequivalent forms of PCB in equal proportions in the microcrystal.

The 2D ^{13}C-^{13}C RFDR MAS NMR spectrum of the u-[^{13}C,^{15}N]-PCB has been recorded in order to separate and assign the carbon resonances (Fig.

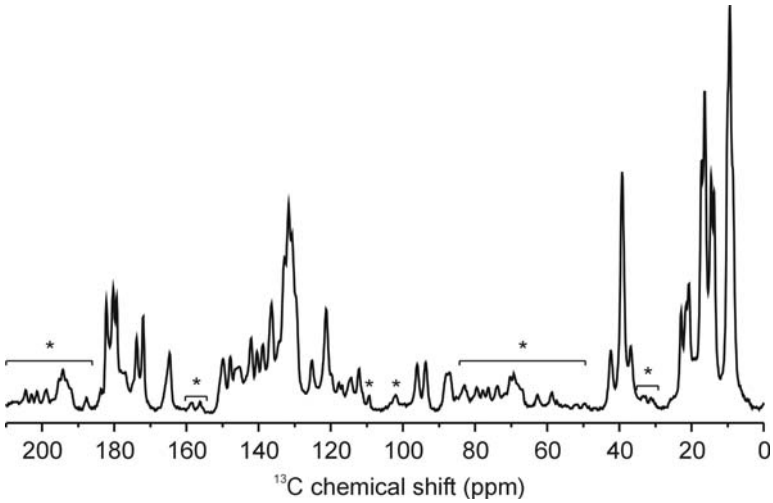

Figure 2.2: 1D ^{13}C CP/MAS NMR spectrum of PCB obtained at 17.6 T, 277 K and 11800 Hz. The asterisks indicate the spinning sidebands.

2.3). The 2D spectra unambiguously confirm the presence of two PCB forms, named A and B, in the microcrystal (Table 2.1). To illustrate the assignment procedure, the correlation network of the A form of the PCB spin system is indicated in Figure 2.3. The resonance at 173.7 ppm, correlating with two aromatic carbons (132.0 and 140.1 ppm) as well as with three aliphatic carbons (10.5, 14.3 and 17.0 ppm), can be assigned in a straightforward manner to the C19 carbon atom of the carbonyl moiety of the ring ***D***. The resonances of the C17 and C18 atoms can be assigned *via* their correlations with the aliphatic carbons atoms. The C16 and C17 spin systems correlate weakly, contrary to the correlations observed for the methine bridge C15, allowing for the assignment of the carbons C16, C15 and C14. For the assignment of the signals in the particularly crowded correlation area of the carbons C11, C12, C13, C14, the cross-peaks with the aliphatic carbons $C13^1$ and $C12^1$ are essential. The correlation peaks of the carbons between C9, C10 and C11 are nicely resolved and provide clear assignments of the carbons forming the C10 methine bridge. The good resolution of the response from the carbon atoms of rings ***A*** and ***B*** (C1 to C9) allows for the unambiguous assignment of the resonances. The signals of C1/C2 were resolved from $C8^2$/$C8^3$ and $C12^2$/$C12^3$ by the correlations with $C2^1$, C3 and C4. Finally, the correlation network between the aromatic and the side-chain carbons is shown in the up-

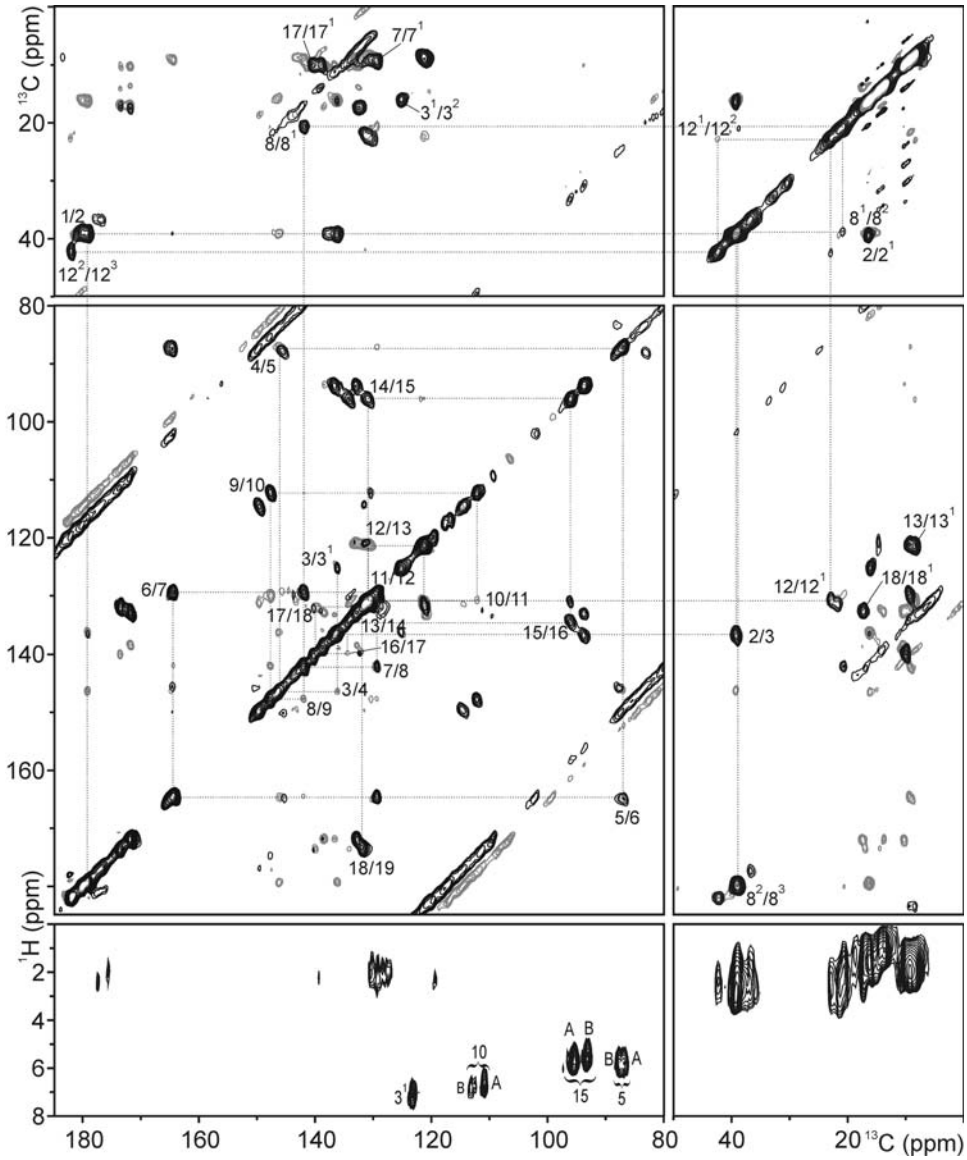

Figure 2.3: The upper panels show the contour plots of ^{13}C-^{13}C RFDR MAS NMR spectrum of u-[^{13}C,^{15}N]-PCB recorded in a field of 17.6 T using spinning frequencies of 11800 Hz (black) and 12500 Hz (grey), and mixing times of 1.8 ms and 3.2 ms, respectively. The lower panels represent the contour plot of the ^{1}H-^{13}C FSLG MAS NMR dipolar correlation spectrum at a spinning frequency of 11800 Hz.

Position	σ_{liq}	σ_A	σ_B	σ_B-σ_A
C1	181.0	179.4	180.3	0.9
C2	39.0	39.3	39.0	-0.3
$C2^1$	15.8	16.3	16.3	0.0
C3	136.7	136.2	137.5	1.3
$C3^1$	124.3	125.2	125.2	0.0
$C3^2$	14.8	16.1	16.1	0.0
C4	147.6	146.2	147.3	1.1
C5	88.5	87.1	88.0	0.1
C6	166.1	164.7	165.6	0.9
C7	132.4	129.5	130.5	1.0
$C7^1$	9.4	9.3	8.7	-0.6
C8	144.8	142.1	143.3	1.2
$C8^1$	21.7	20.7	18.8	-1.9
$C8^2$	38.8	38.6	36.6	-2.0
$C8^3$	179.3	180.5	177.7	-2.8
C9	n.d.	147.8	149.5	1.7
C10	113.4	112.2	114.5	2.3
C11	133.2	130.6	131.5	0.9
C12	134.8	130.8	131.4	0.6
$C12^1$	21.4	22.8	21.6	-1.2
$C12^2$	38.5	42.4	39.6	-2.8
$C12^3$	179.1	182.2	181.7	-0.5
C13	125.1	121.3	121.0	-0.3
$C13^1$	8.8	8.4	9.2	0.8
C14	133.2	131.1	133.0	1.9
C15	98.3	96.0	93.6	-2.4
C16	138.3	134.3	136.7	2.4
C17	142.9	140.1	138.6	-1.5
$C17^1$	9.3	10.5	10.3	-0.2
C18	133.8	132.0	132.8	0.8
$C18^1$	17.3	17.0	17.3	0.3
$C18^2$	13.3	14.3	13.7	-0.6
C19	176.0	173.7	172.0	-1.7

Table 2.1: ^{13}C chemical shifts of PCB in CD_3OD solution (σ_{liq}) and of the two sets of signals observed in the solid-state (σ_A and σ_B).

per left and middle right panels. The high resolution of these signals allows for the assignments of most of the side-chain carbon atoms. However, the correlation peaks of the carbon atoms of the propionic acid side-chains are poorly resolved in the RFDR spectrum.

A PDSD spectrum was collected to resolve the correlation networks of the propionic acid side-chain carbons (Fig. A.2). The resolution of the correlation signals is improved by the PDSD sequence and all side-chain carbon atoms can be unambiguously assigned (Table 2.1). Interestingly, the correlation peaks of the pyrrole rings ***A*** and ***B*** of the B form, in particular for the carbon

atoms C1 to C8, are significantly broader than the corresponding signals of the A form. The correlation peaks may be affected by dynamics, suggesting different mobility in the region of pyrrole rings ***A*** and ***B***.

The 2D frequency-switched Lee-Goldburg heteronuclear ^{1}H-^{13}C correlation spectrum of the u-[^{13}C,^{15}N]-PCB using a CP contact of 256 μs is presented in the lower panels of the Figure 2.3. Spectra obtained with CP contact times of 512 and 1024 μs are shown in Appendix A (Figs. A.3A and B, respectively). In the left panel, the proton resonances correlating with the methine bridge carbons are readily resolved. In line with the doublings observed for the carbon response, also the proton signals exhibit different chemical shifts in the A and B forms (Table 2.2). The chemical shifts of the protons bound to the carbon atoms C10 (6.4 and 6.6 ppm) and C15 (5.5 and 5.3 ppm) are clearly different in the A and B forms, while the protons attached to the carbons C3^{1} and C5 exhibit a similar chemical shifts in both A and B forms (6.8 and 5.5 ppm, respectively). Moreover, the H10 ^{1}H-^{13}C correlation signal of the A form is more intense than in the B form, suggesting that the proton at C10 has a different ^{1}H environment in A and B forms. The correlations with saturated carbons are depicted in the right panel. The small ^{13}C chemical shift dispersion of the methyl groups results in strongly overlapping signals, which cannot be assigned.

2.2.2 ^{15}N chemical shift assignment

The ^{15}N CP/MAS spectrum of u-[^{13}C,^{15}N]-PCB is shown in Figure 2.4. Three strong resonances at 154.2, 150.4, 133.1 ppm are dominating. Due to their chemical shifts and their anisotropy pattern with modest sideband intensities, these three signals originate from protonated nitrogen atoms [83,84]. On the other hand, the centerband resonance at 260.8 ppm having much lower intensity arises from an unprotonated nitrogen atom. The anisotropy pattern of this signal shows intense spinning sidebands. Contrary to the carbon spectra, the ^{15}N resonances are not clearly split. However, the peak at 154.2 ppm exhibits a shoulder, which can be resolved by Lorentzian deconvolution as a signal at 156.9 ppm. The two other resonances of protonated nitrogen atoms can be fitted sufficiently with a single Lorentzian function (data not shown).

The 2D ^{15}N-^{13}C correlation spectrum of u-[^{13}C,^{15}N]-PCB is shown in Figure 2.5. ^{15}N-^{13}C heteronuclear correlations obtained by a double CP experiment allow to assign the ^{15}N resonances using the ^{13}C assignment (Table

Position	σ_{liq}	σ_A	σ_B	σ_A-σ_B
H2	3.21	n.d.	n.d.	
$H2^1$	1.34	n.d.	n.d.	
$H3^1$	6.54	6.8	6.8	0.0
$H3^2$	1.93	1.9	1.9	0.0
H5	5.99	5.5	5.5	0.0
$H7^1$	2.08	1.8	1.8	0.0
$H8^1$	2.93	2.1	1.4	0.7
$H8^2$	2.43	n.d.	n.d.	
$H8^3$	n.d.	n.d.	n.d.	
H10	6.96	6.4	6.6	-0.2
$H12^1$	2.98	2.0	2.7	-0.7
$H12^2$	2.45	2.3	n.d.	
$H12^3$	n.d.	n.d.	n.d.	
$H13^1$	2.16	n.d.	n.d.	
H15	6.14	5.5	5.3	0.2
$H17^1$	2.14	1.7	1.6	0.1
$H18^1$	2.30	1.4	1.5	-0.1
$H18^2$	1.09	1.1	0.8	0.3

Table 2.2: ^{1}H chemical shifts of PCB in CD_3OD solution (σ_{liq}) and of the two sets of signals observed in the solid state (σ_A and σ_B).

2.3). The ^{15}N-^{13}C heteronuclear correlation peaks allow for an unambiguous assignment of all nitrogen atoms. The up-shifted signal at 133.1 ppm is assigned to nitrogen N24, as shown by the correlation to the carbons C16 and C19. Similarly, the resonances at 150.4 and 154.2 ppm are assigned to N23 and N21, respectively. The signal at 260.8 ppm is attributed to nitrogen N22, revealing that the unprotonated nitrogen is located at the ring ***B*** of the tetrapyrrole moiety.

Finally, the 2D ^{1}H-^{15}N heteronuclear correlation FSLG spectrum of the u-[^{13}C,^{15}N]-PCB has been recorded (Fig. A.4). The hydrogens bound to N21 and N24 exhibit chemical shifts at 12.2 and 11.2 ppm, respectively, while the proton bound to N23 is slightly upshifted at 10.7 ppm.

Despite the presence of the shoulder at 156.9 ppm, no correlation peak was found at this frequency neither in the ^{1}H-^{15}N nor in the ^{15}N-^{13}C heteronuclear correlation spectrum. The ^{13}C signals of the ring ***A*** are broad in the B form. The ^{15}N signal at 156.9 ppm may arise from N21 of the PCB moiety in the B form. The slightly different ^{15}N chemical shifts of N21 in the A and B forms may be due to a different geometry of the ring ***A*** and/or a different hydrogen-bonding interaction of this nitrogen in the B form.

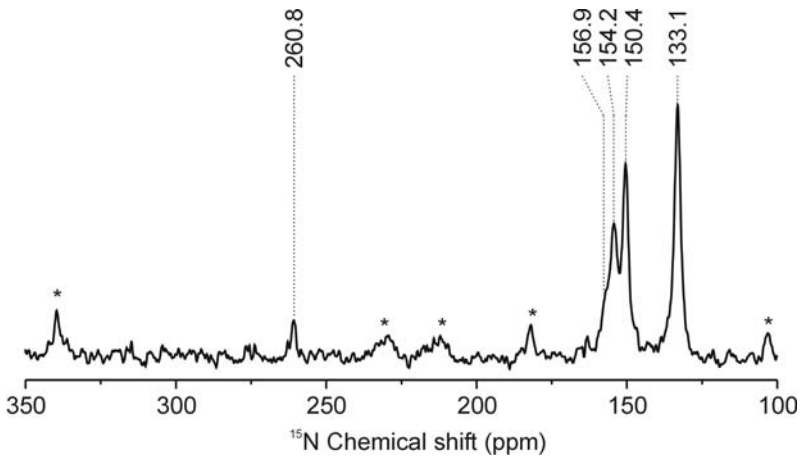

Figure 2.4: ^{15}N CP/MAS NMR spectrum of u-[^{13}C,^{15}N]-PCB recorded at 277 K in a field of 17.6 T using a spinning frequency of 7 kHz. The spinning sidebands are indicated with asterisks.

2.3 Discussion

2.3.1 PCB tautomers

The ^{15}N CP/MAS NMR spectrum of PCB reveals that three nitrogen atoms are protonated. For asymmetrically substituted bilin derivatives, such partitions of acidic hydrogen atoms bound to nitrogen lead to a total of twenty potential tautomers (four bis-lactam, twelve *mono*-lactam and four *bis*-lactim forms). The 2D ^{15}N-^{13}C correlation spectrum in Figure 2.5 demonstrates that both outer ring nitrogens, *i.e.*, N21 and N24, are protonated. Hence, the PCB molecules are in a *bis*-lactam state and the potential tautomerization modes are restrained to the dipyrrin types of tautomerization involving the nitrogens of rings ***B*** and ***C***. It has been shown that PCB-like compounds adopt a helical conformation in which the inner (N$\cdots$H—N) hydrogen-bonding plays a predominant role in the stabilization of the molecular structure [85, 86]. On the other hand, the tautomerism within the central rings of asymmetrically substituted 1,19-dioxobilin, *i.e.*, either the N22$\cdots$H—N23 or the N22—H$\cdots$N23 tautomer, is still under debate [77, 87–89]. The ^{13}C and ^{15}N CP/MAS NMR data shown in this chapter (Figs. 2.3 and 2.5) allow for an unambiguous assignment of all nitrogens of PCB and show that the pyrrolenine nitrogen atom is exclusively placed on the inner ring ***B***.

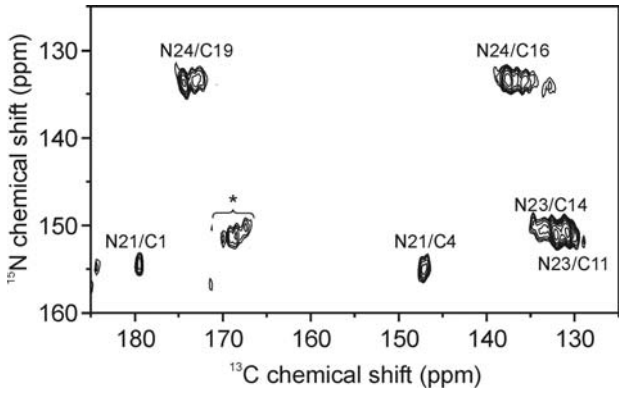

Figure 2.5: Contour plot of the 2D ^{15}N-^{13}C heteronuclear dipolar correlation spectrum of u-[^{13}C,^{15}N]-PCB recorded at 277 K in a field of 17.6 T using a spinning frequency of 8 kHz. The spinning sidebands are indicated with asterisks.

2.3.2 Differences between forms A and B

The ^{13}C NMR study of PCB in its microcrystalline state reveals the presence of two PCB forms in the microcrystal. The differences in the ^{13}C chemical shifts are mainly observed around the C10 and C15 methine bridges and at both of the propionic acid side-chains, while only little variation in ^{13}C chemical shift was detected for the C1 to C7 region of the molecule (Fig. 2.1). In addition, the resolved proton signals for the hydrogens at the C3^1 and C5 positions exhibit the same chemical shift in both A and B forms. Unlike the H3^1 and H5, the H10 and H15 protons show some difference in their chemical shifts (0.20 and 0.15 ppm, respectively, Table 2.2). Taking the ^{13}C and ^{1}H chemical shift variation between A and B forms into account, it can be concluded that PCB adopts two geometries in the microcrystal. The geometry of the ring ***A*** and the C5 methine bridge appear similar in both forms A and B, while the remaining parts of PCB are probably distinguished by the torsional angles about the single bonds at the methine bridges C10 and C15.

In addition to steric constraints, hydrogen-bonding may play an important role in the stabilization of a specific conformation. Due to the presence of the two carboxylic groups at the C8^3 and C12^3 positions, hydrogen-bonds between the propionic acid chains are possible. The pronounced ^{13}C chemical shift variations observed at the propionic acid side-chain, in particular at

Position	σ_{liq}	$\sigma_{A/B}$
N21	157.9	154.7
N22	245.5	260.8
N23	153.0	150.3
N24	131.3	133.1

Table 2.3: ^{15}N chemical shifts of PCB in CD_3OD solution and solid state.

the C8^2, C12^1, C12^2 and C12^3 positions, suggest conformational differences originating from different hydrogen-bonding networks between the carboxylic groups. Finally, the broad ^{13}C resonances of the carbon atoms C8^1 and C12^3 of the B form suggest a high mobility of these side-chains.

2.3.3 PCB Dimers

X-ray crystallographic analyses of open-chain tetrapyrroles like 2,3 dihydrobilatriene-abc derivatives [90, 91] and biliverdin dimethylester [85] have shown that these compounds form dimers in the crystalline state. The dimers are stabilized by intermolecular hydrogen-bonding interactions between the N–H and C=O groups of the outer pyrrole rings. In the case of PCB, the ^{13}C NMR data show unambiguously that the two A and B forms are present in equal ratio in the microcrystal. The comparison of the ^{13}C chemical shifts of PCB obtained by liquid-state and solid-state NMR suggests that the helical (all-*Z*, all-*syn*)-geometry is conserved in both A and B forms in the microcrystal. In addition, it has been suggested that dimerization of PCBE occurs in solution [74, 89]. Despite the different terminal group of the side-chain at C8 and C12 in PCB (acid) and PCBE (ester), there is converging evidence that the dimerization is likely to occur for PCB in the solid state.

The formation of intermolecular N—H$\cdots$C=O hydrogen-bonds may play a role in the stabilization of PCB in a specific geometry. Four types of dimers involving intermolecular hydrogen bonds between the outer rings can potentially be formed (***A***–***A***', ***D***–***D***', ***A***–***D***' and ***D***–***A***').

It is known that the helical structure of 1,19-dioxobilins are determined by the hydrogen-bonding interaction between the unprotonated inner ring nitrogen and the hydrogen atoms of two close-by protonated nitrogen atoms [77]. It has been shown in section 2.2.2 that N22 is unprotonated in both A and B forms. Hence, in the case of PCB, this interaction is of the form N21—H$\cdots$N22$\cdots$H—N23. Thus, dimerization involving the rings ***D*** is the

most likely to occur.

2.3.4 Geometry optimization and dimer characterization

Quantum chemical density functional theory (DFT) calculations using the B3LYP exchange-correlation functional [92] in combination with the 6-31G* basis set [93] have been used for geometry optimization (Dr. Franz Mark, personal communication). The DFT study reveals the existence of two low-energy families of PCB dimers. The first family of dimers involves hydrogen-bonding interactions between the rings ***D*** and ***D***' (Fig. 2.6A). One of the subunits in the dimers forms a **P** helix, the other an **M** helix. The two PCB moieties are bound together by means of two hydrogen-bonds (N24—H$\cdots$O19' and O19$\cdots$H'—N24') with distances of 2.83 and 2.88 Å. Small differences in torsional angles of the double and single bonds at the C15, C10 and C5 methine bridges are due to the intermolecular steric interactions. Hence, the two monomers have a similar helical shape but are not symmetric.

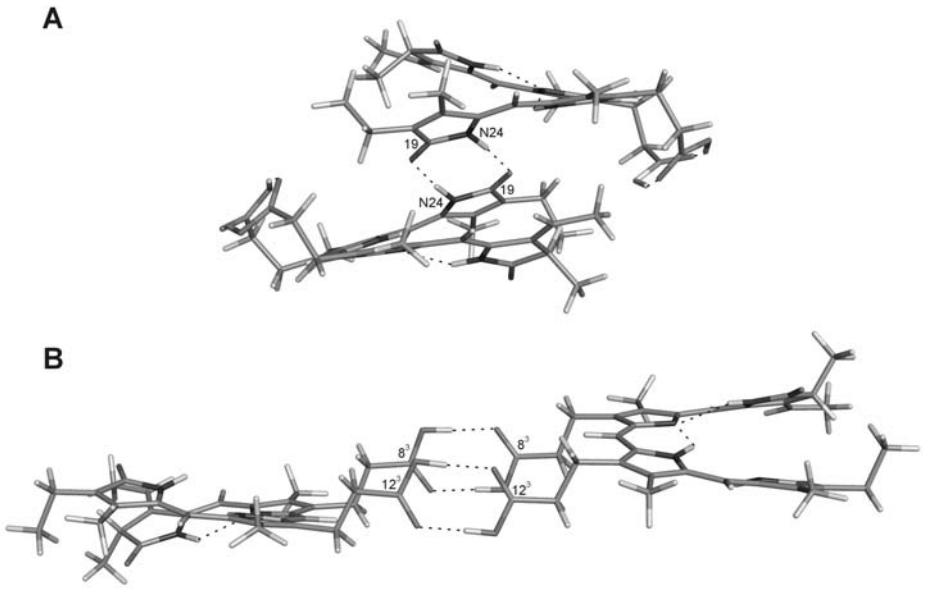

Figure 2.6: View of the low-energy families of dimers ***D***–***D***' (**A**) and P–P' (**B**) obtained by geometry optimization at the B3LYP/6-31G* level of theory.

The formation of the second lowest-energy family of dimers, called P–P', occurs *via* the propionic side-chains of the PCB molecules. Hence, the geometry of the three methine bridges of each monomer P is solely governed by the intramolecular hydrogen-bonding system N21—H$\cdots$N22$\cdots$H—N23 and by the intramolecular steric interactions between its side-chains without being significantly affected by the other monomer P'. In the lowest-energy P–P' dimer, the two subunits are composed of two enantiomeric **M** helical monomers (Fig. 2.6B).

Due to the enantiomeric relation between the P and P' monomer, the NMR spectrum of this family would consist of a unique set of chemical shifts. On the other hand, the two slightly different monomers found in the ***D***–***D***' family would generate two sets of chemical shifts. Since the MAS NMR analysis of PCB in its microcrystalline state demonstrates the presence of two forms, it is most likely that the two sets of chemical shifts are due to the occurrence of the ***D***–***D***' family of dimers in the crystal.

2.4 Materials and methods

2.4.1 Sample preparation

Uniformly [^{13}C,^{15}N]-labeled PCB was obtained by growing axenic cultures of *Synechocystis* sp. PCC 6803 cells at room temperature in a modified BG11 medium under constant illumination with continuous white light [94]. Cells reached a stationary phase after 3-4 weeks ($OD_{750} \sim 3$) and were harvested by centrifugation at 5000g for 20 min at 4 °C. The pellet was resuspended in 30 mL of 0.75 M K_nPO_4 buffer (pH 7) and 5 mM EDTA (pH 8), and broken with a French press (two passages, 21500 N). The cellular debris was pelleted at 25000g for 30 min at 4 °C. Ammonium sulfate was added to the supernatant (3/2, v/v) and the sample was spun in a swing-out rotor for 20 min at 5000 rpm (4 °C). The pelleted sample was washed with 30 mL of ice-cold methanol and centrifuged at 5000 rpm for 10 min. Pellets were resuspended in methanol (1/15, v/v), incubated 18 h at 54 °C, and centrifuged (15 min, 5000 rpm, 4 °C). The supernatant was collected and concentrated to 5 mL. The residue was purified by reverse-phase HPLC using published procedures [46].

2.4.2 Mass spectrometry

The ^{13}C and ^{15}N isotope enrichments were measured by mass spectrometry. PCB was diluted in methanol containing 1% acetic acid. The mass spectrum was acquired in positive ion mode by direct infusion (5 $\mu L \cdot min^{-1}$) using a LTQ FT hybrid mass spectrometer (ThermoFischer, Bremen, Germany) equipped with an electrospray ionization source. The capillary was typically held at 3.5 kV, the transfer capillary was maintained at 280 °C and the tube lens was set to 240 V. 15 scans were accumulated for each experiment. A ^{13}C and ^{15}N isotope enrichment of about 90% has been deduced from the mass spectrum.

2.4.3 NMR experiments

For the MAS NMR measurements, about 2 mg of u-[^{13}C,^{15}N]-PCB was placed into a 4-mm CRAMPS rotor. All MAS NMR experiments were performed at 277 K with an Avance 750 spectrometer (Bruker BioSpin, Karlsruhe, Germany), equipped with a triple-resonance MAS probe head and operating at a resonance frequency of 750.1 MHz for ^{1}H, 188.6 MHz for ^{13}C and 76.0 MHz for ^{15}N. RFDR and PDSD pulse sequences were used to record ^{13}C-^{13}C homonuclear correlations. For both 2D experiments, proton $\pi/2$ pulses were set to 3.1 μs and a CP contact time of 2.0 ms was used. A ramped CP sequence (100-80%) with a cycle delay of 1 s was applied. Heteronuclear two-pulse phase modulation decoupling was applied during acquisition [65]. For the RFDR experiment, a continuous wave decoupling of 80.6 kHz was used to decouple the protons during the mixing time. For the PDSD experiment, the proton decoupling was switched off during the spin diffusion mixing period to obtain ^{1}H-mediated transfer of ^{13}C polarization along the molecular network. Heteronuclear ^{1}H-^{13}C and ^{1}H-^{15}N correlations were obtained by FSLG experiments using short CP times of 256 μs and a ^{1}H $\pi/2$ pulse length of 3.1 μs. The ^{1}H chemical shift scale was calibrated from a FSLG spectrum of solid tyrosine·HCl salt.

^{15}N-^{13}C double CP/MAS spectrum of u-[^{13}C,^{15}N]-PCB was recorded with the same spectrometer using a triple resonance CP-MAS probe head with a spinning rate of 8 kHz. ^{15}N polarization was created with a 80-100% ramped amplitude CP matching and a contact time of 2.0 ms. During ^{15}N evolution TPPM decoupling with a RF field strength of 81 kHz was used. For the CP transfer from ^{15}N nuclei to the ^{13}C aromatic carbons, the ^{15}N carrier

frequency was placed at 143 ppm [95]. During the dipolar contact time of 2.0 ms for the ^{15}N-^{13}C transfer, a weak RF field of 22.5 kHz for ^{15}N was employed. The RF field strength for ^{13}C was 31 kHz for the ^{15}N-^{13}C band selective CP. During the ^{15}N-^{13}C transfer, continuous wave decoupling was applied at the ^{1}H frequency. TPPM was employed for decoupling during acquisition. ^{15}N chemical shifts were referenced to liquid ammonia with use of an external standard of ^{15}N-glycine (34.3 ppm).